J Mater Sci (2007) 42:8254–8261
DOI 10.1007/s10853-007-1616-8

Structural and electrical properties of zinc-substituted cobalt ferrite

Wafaa Bayoumi

Received: 14 December 2006 / Accepted: 14 February 2007 / Published online: 10 July 2007

Abstract Polycrystalline samples of $Co_{1-x}Zn_xFe_2O_4$ with stoichiometric proportion (x) varying from 0.0 to 1.0 were prepared through the thermal decomposition of their respective oxalates. The samples were calcined at 1000 °C for 3 h and characterized using X-ray diffraction (XRD) and Mössbauer spectroscopy techniques. The study of the cation distribution using Mössbauer spectroscopy showed that the ions at the tetrahedral site moved to the octahedral site by the addition of zinc and that the system varied from an inverse to a normal spinel structure. The values of the lattice parameter, X-ray density, oxygen parameter, inversion factor and radii of tetrahedral and octahedral sites were calculated using X-ray diffraction data. The temperature dependence of the conductivity showed a definite kink, except for the $ZnFe_2O_4$ sample, which can be attributed to the ferromagnetic–paramagnetic transitions. The calculated activation energy in the paramagnetic region was found to be smaller than that in the ferromagnetic region.

Introduction

The study of transition metal oxides, especially spinel ferrites which have vast applications from microwave to radiowave frequencies, is of great importance from both fundamental and applied research point of view [1] the characteristic physical properties of the spinel ferrites, as electrical conductivity, dielectrical constant, thermoelectrical power, magnetic and catalytic properties, responsible for their application in various fields, arise from the ability of these compounds to distribute the cations amongst the available two sublattices, tetrahedral (A) and octahedral (B) sites [2]. The factors related to the ionic charge and radius, crystal and ligand fields and anion polarization play an important role in the site preference of cations. Ferrites [3] are capable of crystallizing in either of two structures: the normal spinel or inverse one. In the normal spinel (such as $ZnFe_2O_4$), zinc ions are located in the tetrahedral site and are symmetrically surrounded by four O^{2-} ions. In the inverse spinel (like $CoFe_2O_4$), half of Fe^{3+} ions are located in the tetrahedral positions whereas the other half are in the octahedral positions. Therefore, a normal ferrite can be described as $(M^{2+})[Fe_2^{3+}]O_4$ and an inverse ferrite as $(Fe^{3+})[M^{2+}Fe^{3+}]O_4$. X-ray diffraction and Mössbauer spectroscopy techniques have been devised to study the cation distribution in spinel ferrites and generally, the cation distribution calculated from X-ray intensity data agrees well with the Mössbauer results [4].

The presence of nonmagnetic ions in spinel was found to alter their magnetic and electrical properties, and studies have revealed useful information on the nature of the exchange interaction, cation exchange, direction of magnetization, etc. Such isomorphous substitution in iron oxides are apparent in their Mössbauer spectra, since these will drastically reduce magnetic interactions, resulting in lower magnetic ordering temperature and decreases magnetic field super transfer [5].

Reddy et al. [6] have been studied the thermoelectric power and electrical conductivity of zinc-substituted cobalt ferrites, prepared by double sintering ceramic technique, as a function of composition and temperature. On the basis of seebeck coefficient, these ferrites can be classified as n-type or p-type semiconductors. The electrical conductivity was found to increase with increasing temperature

W. Bayoumi (✉)
Chemistry Department, Faculty of Science, Benha University, Benha, Egypt
e-mail: wafaa_bayoumy@hotmail.com

with a change of the slope at magnetic transition. The values of charge carrier concentration and mobility are also computed and discussed. An attempt was made also to explain the conduction mechanism in these ferrites.

Duong et al. [7] have been prepared zinc substituted cobalt ferrite powders using forced hydrolysis method. Magnetic and structural studies for these specimens showed that, they have an average crystallite size of about 3.0 nm with super paramagnetic properties at temperatures below the blocking temperature.

Reddy et al. [8] have been measured the high-frequency dielectrical behavior of polycrystalline zinc substituted cobalt ferrites. The dielectric constant of these ferrites was found to be approximately inversely proportional to the square root of the resistivity and shows a transition near the Curie temperature.

Gul et al. [9] have been prepared nanoparticles of $Co_{1-x}Zn_xFe_2O_4$ with stoichiometric proportion (x) varying from 0.0 to 0.6 by the chemical coprecipitation method. The samples were characterized by X-ray diffraction (XRD), low field AC magnetic susceptibility, DC electrical resistivity and dielectric constant measurements. It was observed that the Curie temperature decreases with the increase of Zn concentration. The DC results are discussed in terms of polaron hopping model. The dielectric constant was found to decrease with increasing frequency for all the samples and follow the Maxwell–Wagner's interfacial polarization.

The present communication was attempts to prepare zinc-substituted cobalt ferrites through the thermal decomposition of their corresponding metal oxalates. The main aim is to understand the effect of diamagnetic substitution of zinc ions on structural, electrical and magnetic properties of cobalt ferrite.

Experimental procedure

Materials and preparation procedure

The starting materials were solids of $CoC_2O_4{\cdot}2H_2O$, $ZnC_2O_4{\cdot}2H_2O$ and $FeC_2O_4{\cdot}2H_2O$. These metal oxalates were prepared by precipitation from aqueous solution of their salts sulfate using analytical grade oxalic acid. For the preparation of the mixed metal oxalates, seven mixtures of these respective metal oxalates with calculated mole ratios, equivalent to the formation of $Co_{1-x}Zn_xFe_2O_4$ ferrite system ($x = 0.0$, 0.1, 0.3, 0.5, 0.7, 0.9 and 1.0) after their thermal decomposition, were prepared by the impregnation technique previously described [10].

Mixed Co–Zn ferrites, $Co_{1-x}Zn_xFe_2O_4$ ($0 \leq x \leq 1$), were prepared by annealing the oxalates mixtures in a muffle furnace at 1000 °C for 3 h under static air atmosphere. Then, the samples were quenched to room temperature and kept in desiccator.

Characterization techniques

DTA–TG behavior of mixed oxalates was investigated using a Shimadzu DT-60 thermal analyzer (Japan). The temperature was raised up to 1000 °C under 1 atm pressure in air flow (30 mL min^{-1}) at heating rate of 5 °C min^{-1}. α-Al_2O_3 powder (Shimadzu) was used as the reference material for DTA measurements and the sample weight in the PT-cell was about 10 mg.

X-ray powder diffraction measurements were obtained using a Philips PW 1370 diffractometer at ambient temperature using monochromated Cu–Kα_1 radiation ($\lambda = 1.5406$ Å).

Mössbauer spectra of the ferrite samples were measured with a time mode spectrometer, calibrated with a high purity natural iron foil of 10 mg cm^{2-} thickness, using a constant acceleration deriver and personal computer analyzer (PCAII-card) coupled to a 1024 multichannel analyzer. A 50 mCi ^{57}Co in Rh matrix was used as the radioactive source. Experimental data were analyzed using the least square fitting ''Mos-90'' computer program [11].

For electrical properties measurements, the ferrite samples in a powdered form were compressed to pellets of 1 cm diameter and about 1 mm thickness. The pressure used was 2 tons cm^{-2}. After calcining the pellets at 900 °C for 2 h, the two surfaces of each one were polished and coated with silver paint (BDH) and tested for Ohmic contact. The real part of the dielectric constant ($\varepsilon^{'}$) and ac conductivity were measured, by a Hioki LCR bridge model 3530 (Japan) using the two probe method [12], at different frequencies (10–5000 kHz) as a function of temperature. The temperature of the sample was measured using a thermocouple type K which is connected to a digital thermometer.

Results and discussion

Thermal decomposition studies of the oxalate mixtures

Figure 1 shows a typical DTA–TG curves for the thermal decomposition of $CoC_2O_4{\cdot}2H_2O$–$ZnC_2O_4{\cdot}2H_2O$–$FeC_2O_4{\cdot}2H_2O$ (with 0.5:0.5:2 molar ratios) in air. From the figure it is clear that the decomposition of the mixture proceeds through five well-defined TG steps and amounts to a total weight loss of 56.2% of its molecular mass at 390 °C which closely corresponds to the formation of mixed of cobalt, zinc and iron oxides. The DTA curve shows peaks which are closely correspond to the weight loss obtained on TG curve. The first two steps are attributed to the complete dehydration of the

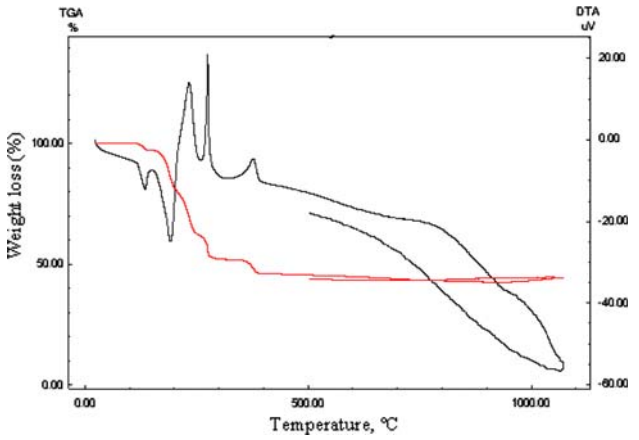

Fig. 1 DTA–TG curves of $CoC_2O_4{\cdot}2H_2O$–$ZnC_2O_4{\cdot}2H_2O$–$FeC_2O_4{\cdot}2H_2O$ (0.5:0.5::2 mole ratios) mixture in air at a specified heating rate of 5 °C min^{-1}

mixture. Two endothermic DTA peaks are characterizing these two steps with peaks temperature at 135, 191 °C. From the calculated weight losses and the dehydration temperatures, the first TG step can be assigned to the dehydration of zinc oxalate content of the mixture and the second one can be attributed to the dehydration of both cobalt and ferrous oxalate content. The third TG step follows immediately after the second one and accompanied by an exothermic DTA peak at 232 °C. This peak is assigned to the oxidative decomposition of ferrous oxalate with the formation of Fe_2O_3 [13]. In the fourth TG step, the cobalt oxalate content of the mixture was found to decompose exothermically (sharp DTA peak at 275 °C). The obtained weight loss in this step agrees well with the formation of CoO. Zinc oxalate content of the mixture was also found to decompose exothermically in the last step (DTA peak at 377 °C) with the formation of zinc oxide. No further changes were observed by raising the temperature up to 1000 °C or by cooling up to about 500 °C.

Characterization of $Co_{1-x}Zn_xFe_2O_4$

X-ray powder diffraction

As can be seen from they XRD patterns (Fig. 2), the investigated samples of $Co_{1-x}Zn_xFe_2O_4$ revealed a cubic spinel structure without any ambiguous reflections. The average particle size of the samples calculated by Scherrer formula [14] was found to be within the range of 100–130 nm. The lattice constant (a) and the X-ray density (D_x) [15] as a function of Zn concentration are tabulated in Table 1. As can be shown in Fig. 3a The lattice parameter; a was found to exhibit a linear content dependence, thus obeying the Vegard's law [16] and since the ionic radius of Zn^{2+} (0.57 Å) is slightly higher than that of Co^{2+} (0.56 Å),

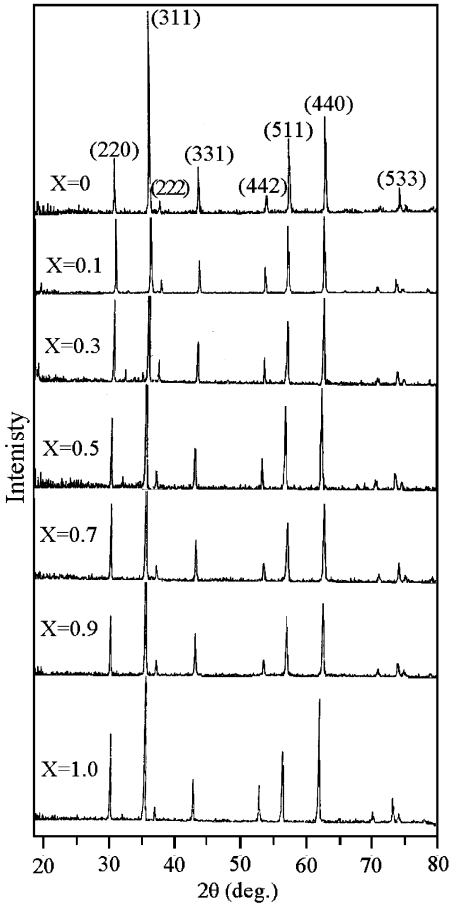

Fig. 2 Characteristic parts of XRD patterns of $Co_{1-x}Zn_xFe_2O_4$ system

the replacement of cobalt by zinc ions leads to an increase of the lattice parameter.

The X-ray density (D_x) values reported in Table 1 was found to increase with increasing x (Fig. 3b). This was expected since the larger zinc atom is heavier than the smaller cobalt atom, and this increase in weight and decrease in size causes an increase in X-ray density.

Table 1 Lattice parameters and X-ray densities of $Co_{1-x}Zn_xFe_2O_4$ system

Zn content (x)	Lattice parameter, a (Å)	D_X (gm cm^{-3})
0.0	8.475	5.119
0.1	8.477	5.129
0.3	8.489	5.134
0.5	8.504	5.136
0.7	8.511	5.150
0.9	8.521	5.159
1.0	8.527	5.162

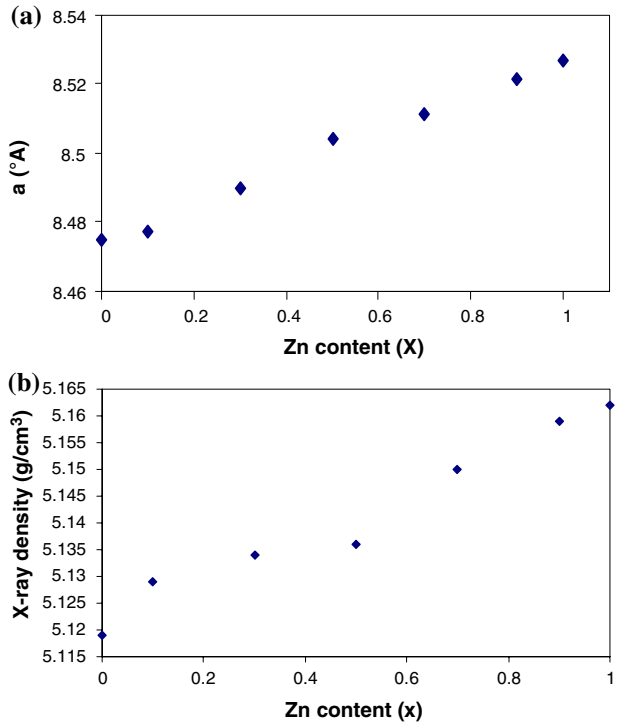

Fig. 3 (**a**) Variation of lattice parameter (*a*) as a function of Zn content and (**b**) Variation of X-ray density (*D*x) with composition

Mössbauer spectroscopy

Figure 4 shows the Mössbauer spectra of Zn–Co ferrites obtained at room temperature. The spectral parameters [isomar shift (δ), quadrupole splitting (ΔE_Q), line width (Γ) and hyperfine magnetic field (*Hn*)] are summarized in Table 2.

For the samples with $x = 0.0$–0.3, the spectra exhibit two normal Zeeman-split sextets due to Fe^{3+} at tetrahedral and octahedral sites, indicating the ferromagnetic behavior of the samples. The solid lines through the data points in Fig. 4 are the results of computer fits of the spectra obtained by assuming equal line width for the *A*- and *B*-sites. The spectrum obtained for the composition with $x = 0.5$ shows features of relaxation effects and was analyzed to a single sextet assigned to the presence of Fe^{3+} ions in the octahedral site (depending on its spectral parameters) and a central paramagnetic doublet resulting from superparamagnetic Fe^{3+} species [17]. From Table 2, it can be observed that the magnitude of magnetic hyper-fine fields of *A* site (H_A) and *B* site (H_B) decrease as the Zn content increases. It can be also observed that, the hyper-fine field of *A* site (H_A) decreases more rapidly than that of *B* site. The rapid decreases of the magnetic hyper-fine field of *A* site as increasing Zn contents is attributed to the dilution of the field component from Fe^{3+} ions in neighboring *A* site.

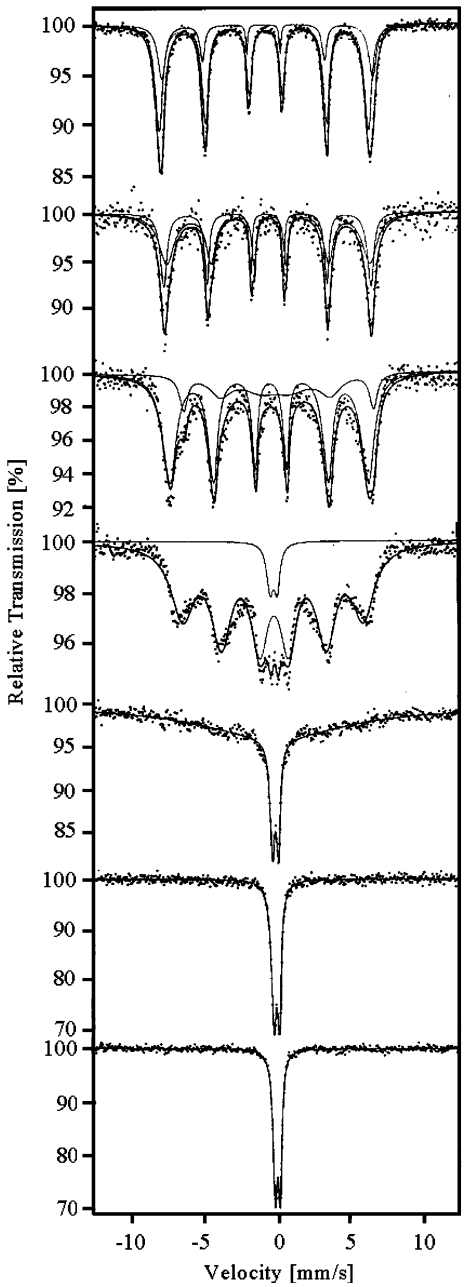

Fig. 4 The Mössbauer spectra at room temperature of $Co_{1-x}Zn_xFe_2O_4$ system

The observed spectra for samples with $x = 0.7$–1.0 consist only of a central doublet. The relative intensity of the central doublet was found to increase with the concentration of Zn^{2+}. The central doublet can be attributed to the magnetically isolated Fe^{3+} ions which do not participate in the long-range magnetic ordering due to a large number of nonmagnetic nearest neighbors.

The fraction of iron ions and consequently the cation distribution at tetrahedral *A* and octahedral *B* sites were determined using the area of Mössbauer subspectra. For

Table 2 Mössbauer parameters of $Co_{1-x}Zn_xFe_2O_4$ system

Zn content (x)	site	Area (%)	Isomer shift (δ) (± 0.02 mm s^{-1})	Quadrupole splitting (ΔE_Q) (±0.02 mm s^{-1})	Line width (Γ mm s^{-1})	Hyperfine field (H_n) (±2 kOe)
0.0	A	73	0.16	0.13	0.61	493
	B	27	0.08	0.27	0.63	497
0.1	A	60	0.03	0.07	1.24	480
	B	40	0.17	0.05	0.53	488
0.3	A	30	0.39	0.22	0.64	452
	B	70	0.17	0.09	1.10	470
0.5	B	–	0.12	0.01	1.86	432
0.7	–	–	0.04	0.11	0.56	–
0.9	–	–	0.09	0.38	0.37	–
1.0	–	–	0.07	0.34	0.33	–

stoichiometric ferrite it is easy to estimate the cation distribution, but it becomes rather difficult for mixed ferrites, since they contain mixtures of more than one cation other than iron. However, if the metal ions have an exclusive preference for any particular site in the spinel, then it is possible to estimate the cation site in the mixed ferrites. For the pure $CoFe_2O_4$ samples, the cation distribution may be described by the chemical formula, $(Co_{0.27}Fe_{0.73})[Co_{0.73}Fe_{1.27}]O_4$, where ( ) denote tetrahedral A sites and [ ] denotes octahedral B sites. For $x = 0.1$ and 0.3, considering that the Zn^{2+} ions prefer A site, and using the area ratio data, we can decide the cation distribution as; $(Co_{0.30}Zn_{0.10}Fe_{0.60})[Co_{0.60}Fe_{1.40}]O_4$ and $(Co_{0.40}Zn_{0.30}Fe_{0.30})[Co_{0.30}Fe_{1.70}]O_4$, respectively. For the samples with $0.5 \leq x \leq 1.0$, according to the obtained spectra, iron completely filled the octahedral site. Consequently, the cation distribution of these samples can be written as reported in Table 3.

Depending on the cation distribution estimated using the Mössbauer spectroscopy, the values of oxygen positional parameter (u) and the degree of inversion (γ) were calculated and summarized in Table 3. For a given spinel compound, the anion sublattice expands or contracts on varying oxygen parameter until the tetrahedral and the octahedral site volumes match the radii of the constituent cations. The oxygen ions are apparently larger than the metallic ions, and in spinel like structure the oxygen parameter has a value of about 0.375 for which the arrangement of O^{2-} ions equals exactly a cubic closed packing, but in actual spinel lattice this ideal pattern is slightly deformed. The higher values of oxygen parameter obtained in our work ($u > 0.375$) may be attributed to the small displacement of anions due to the expansion of the tetrahedral interstices [18]. The inversion parameter (γ), defined as the total fraction of divalent ions lodged in the octahedral site, was found to decrease and going towards complete inversion at $x = 0.5$.

Depending on the cation distribution obtained the radius of the tetrahedral and octahedral sites and intercationic distances were also calculated using experimental values of lattice constant and oxygen parameter for $Co_{1-x}Zn_xFe_2O_4$ system using equations from [15]. The results were reported in Table 3. From the results it is clear that, the radius of the tetrahedral site becomes larger on addition of zinc ions which can be ascribed to the preference of the zinc ions with larger ionic radius for the tetrahedral coordination.

Table 3 Cation distribution, oxygen parameter, inversion parameter and cation–anion distance of $Co_{1-x}Zn_xFe_2O_4$ system

Cation distribution	u	γ	r_A	r_B	tet. bond	oct. bond	tet. edge	oct. edge	
								shared	unshared
$(Co_{0.27}\ Fe_{0.73})[Co_{0.73}Fe_{1.27}]O_4$	0.379	0.7	0.509	0.682	1.894	2.085	3.092	2.901	2.997
$(Zn_{0.1}Co_{0.3}Fe_{0.6})[Co_{0.6}Fe_{1.4}]O_4$	0.379	0.6	0.519	0.675	1.894	2.086	3.093	2.901	2.998
$(Zn_{0.3}Co_{0.4}Fe_{0.5})[Co_{0.5}Fe_{1.5}]O_4$	0.381	0.3	0.542	0.660	1.926	2.069	3.145	2.857	3.003
$(Zn_{0.5}Co_{0.5})[Fe_2]O_4$	0.382	0.0	0.565	0.645	1.944	2.068	3.175	2.838	3.009
$(Zn_{0.7}Co_{0.3})[Fe_2]O_4$	0.382	0.0	0.567	0.645	1.946	2.069	3.178	2.841	3.011
$(Zn_{0.9}Co_{0.1})[Fe_2]O_4$	0.382	0.0	0.569	0.645	1.948	2.072	3.181	2.844	3.015
$(Zn)[Fe_2]O_4$	0.382	0.0	0.570	0.645	1.950	2.074	3.184	2.846	3.017

r_A = tet. radius, r_B = oct. radius

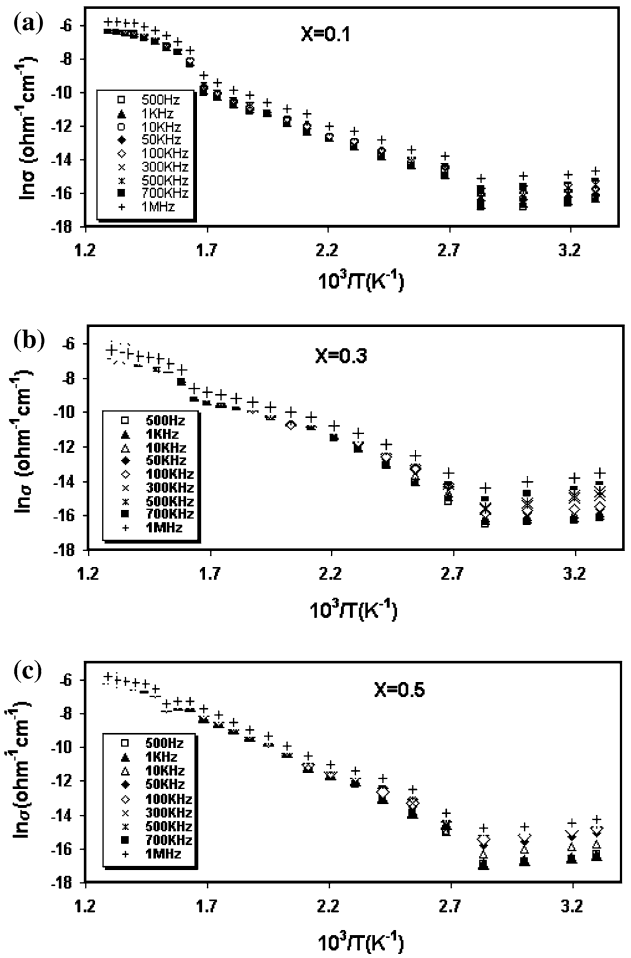

Fig. 5 Relation between lnσ and reciprocal of absolute temperature at different Zn content as a function of applied frequency for $Co_{1-x}Zn_xFe_2O_4$ system

Electrical properties studies

Figure 5a–c show typical curves of the alternative current conductivity versus reciprocal absolute temperature as a function of the applied frequency for the $Co_{1-x}Zn_xFe_2O_4$ system. It can be concluded that the conductivity for all the samples is frequency independent at high temperature regions, while at low temperature region its values slightly changed with changing frequency. On the other hand, the conductivity of all samples was found to be temperature dependent.

From the figure it is clear that four regions intersecting at three transition temperatures are obtained, one of them is distinguished as the Curie point (T_C). The first and the last regions are nearly the same, clarifying the metallic behavior of the investigated samples in the low and very high temperature regions. The thermal energy in the first region is not enough to liberate charge carriers and consequently the conductivity is hardly changed with temperature. In the last region the large thermal energy causes a large lattice vibration and the scattering of the charge carriers due to their collision with the vibrating lattice was expected to damp the mobility up to the extent at which it becomes constant and giving rise to a constant conductivity. In the intermediate region, the conductivity was found to increase with increasing temperature giving a kink in each curve, at temperature which corresponds to ferrimagnetic (ordered state) to paramagnetic transition (disorder state). No such a magnetic transformation was observed for $ZnFe_2O_4$ sample, suggesting that this sample is paramagnetic at room temperature. The low temperature region represents the ferromagnetic region, while the other at high temperature represents the paramagnetic region. The point incorporated between the two regions is assigned to the Curie transition point (T_C).

Table 4 Values of activation energy at applied frequency of 200 kHz for $Co_{1-x}Zn_xFe_2O_4$ system

Zn content (x)	σ at 400 K (Ω^{-1} cm^{-1})	μ_d at 400 K (cm^2 V^{-1} s^{-1})	Activation energy (eV)	
			(E_I)	(E_{II})
0.0	1.2×10^{-5}	3.1×10^{-7}	0.42	0.66
0.1	4.3×10^{-6}	6.7×10^{-8}	0.40	0.53
0.3	2.3×10^{-6}	1.5×10^{-8}	0.38	0.51
0.5	1.7×10^{-6}	2.4×10^{-9}	0.32	0.47
0.7	1.2×10^{-6}	2.7×10^{-10}	0.26	0.42
0.9	9.2×10^{-7}	6.9×10^{-11}	0.22	0.39
1.0	7.1×10^{-7}	1.2×10^{-12}	–	0.37

The electrical conductivity-temperature behavior obeys Wilson's law [19], indicating the semiconducting nature of all the compounds under investigation. The activation energies were calculated for the two regions around the kink, firstly for the ferromagnetic (low-temperature region: E_I) and secondly for the paramagnetic (high-temperature region: E_{II}). The calculated values of the activation energy are listed in Table 4. From the table it is clear that the activation energy in the paramagnetic region is higher than that in the ferrimagnetic one. This result is in agreement with the theory developed by Irkin and Turov [20] For the existence of the kinks or transition in the neighborhood of the Curie point. Generally the change of the slope is attributed to the change in the conductivity mechanism. The conduction at lower temperature (below Curie temperature) can be attributed to hopping of electrons between Fe^{2+} and Fe^{3+} ions and jumping of holes between Co^{2+} and Co^{3+} ions, whereas at higher temperature (above Curie temperature) due to polaron hopping [21]. The calculated activation energies in the paramagnetic region E_{II} are greater than 0.40 eV which clearly suggest that the conduction is due to polaron hopping [8].

The decrease in activation energy calculated for both regions with increasing x can be interpreted as follows [22]: as hopping between atoms of different metals on the octahedral sublattices needs higher activation energy than for ions of the same metals [23] thus, conduction activation energy for $CoFe_2O_4$ is higher (since the octahedral site contains a large ratio of Co^{2+} ions). As can be seen from Table 3, the addition of Zn^{2+} ions leads to an increase of Fe^{3+} ions in the octahedral site and a simultaneous decrease of Co^{2+} ions present at the same site. This will increase ions of the same metal (Fe^{3+} ions) and, consequently, decrease of the conduction activation energy. Also, it can be seen that the conductivity values (taken at 400 K) decrease with increasing zinc content (Table 4). Since a part of the conductivity at this temperature range is attributed to the jumping of holes between Co^{2+} and Co^{3+} ions, thus, the replacement of zinc on the expense of cobalt will consequently decrease this process and, consequently, decrease of the conductivity. The drift mobility for all the samples at 400 K has been calculated using the equation: $\sigma = n\ e\ \mu_d$, where σ is the conductivity, n is the concentration of charge carrier and e is the charge of electron. From Table 4, it can be observed that the drift mobility decrease with the increase of Zn concentration.

Dielectric constant (ε') in ferrites is also contributed by several structural and microstructural factors. The dielectric constant as a function of frequency was determined using the formula:

$$\varepsilon' = Cd/\varepsilon_0 A$$

where C is the capacitance of the pellet in farad, d the thickness of pellet in meter, A the cross-sectional area of the flat surface of the pellet and ε_0 is the constant of permittivity of free space.

Figure 6 shows the variation of dielectric constant with absolute temperature at different frequencies from 500 Hz to 1 MHz. It can be seen that all the samples show the frequency-dependent phenomena i.e. the dielectric constant decreases with increasing frequency. This is a normal behavior observed in most of the ferrimagnetic materials, which may be due to the interfacial polarization as predicted by Maxwell–Wagner [24]. According to Rabinkin and Novikova [25] the polarization in ferrites is through a mechanism similar to the conduction process. By electron exchange between Fe^{2+} and Fe^{3+}, the local displacement of electrons in the direction of the applied field occurs and these electrons determine the polarization. The polarization decreases with increasing frequency and then reaches a constant value due to the fact that beyond a certain frequency of external field, the electron exchange between Fe^{2+} and Fe^{3+} cannot follow the alternating field. The large value of 'ε_0' at lower frequency is due to the predominance

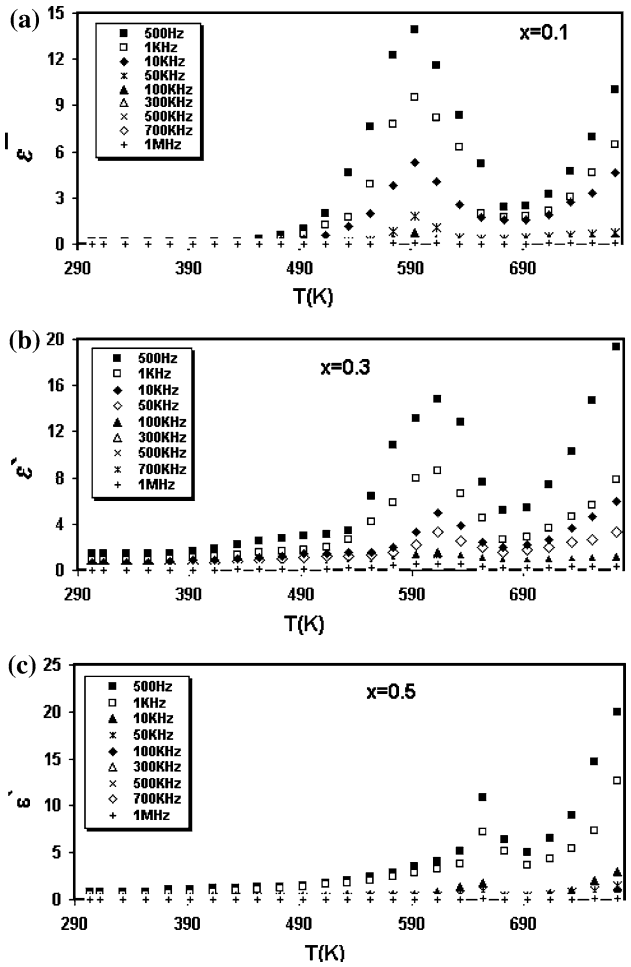

Fig. 6 Relation between dielectric constant and the absolute temperature as a function of applied frequency for $Co_{1-x}Cd_xFe_2O_4$ system

of species like Fe^{2+} ions, interfacial dislocations pile ups, oxygen vacancies, grain boundary defects etc [24].

It is evident that by increasing the temperature, the dielectric constant increases gradually up to the particular point designated as the dielectric transition temperature (T_d) with position depending on the amount of zinc in the sample. This transition is in a good agreement with that obtained in the conductivity measurements. Beyond this temperature, the values of dielectric constant for all samples were found to decrease. Similar behavior has been reported earlier [26]. The behavior of ε' with the temperature can be explained as follows: at relatively low temperature, the charge carriers on most cases cannot orient themselves with respect to the direction of the applied field, therefore, they posses a week contribution to the polarization and the dielectric constant. As the temperature increases, the bound charge carriers get enough excitation thermal energy to be able to obey the change in the external field more easily. This in turn enhances their contribution

to the polarization leading to an increase of the dielectric constant of the sample [27]. The decrease of (ε') is attributed to the decrease in internal viscosity of the system giving rise more degrees of freedom to the dipoles with the result of increasing the disordering in the system and hence decreasing (ε') again.

Conclusion

(1) Zinc-substituted cobalt ferrites were prepared through the thermal decomposition of their respective metal oxalates.
(2) X-ray diffraction of the investigated samples shows single phase cubic spinel.
(3) The lattice parameter was found to increase with the addition of zinc due to the larger ionic radius of Zn compared with that of Co.
(4) The Mössbauer spectra of samples with $x \geq 0.5$ show a paramagnetic doublet while samples with $x \leq 0.3$ exhibit normal Zeeman split sextets. The magnetic hyperfine field was found to decrease with increasing Zn content. The cation distribution of the investigated ferrites was also estimated.
(5) The temperature variation of the electrical conductivity of all the samples excepts for the $ZnFe_2O_4$ sample shows a definite break, which corresponds to ferrimagnetic–paramagnetic transition. The activation energy in the paramagnetic region is higher than in the ferrimagnetic region.

References

1. Murase T, Igarahi K, Sawai J, Nomura T (1999) ICF7. Bordeaux, France
2. Wacrenoborgh JC, Figucerido MO, Cabrol JMP, Pereiro LCJ (1994) J Sol State Chem 111:300
3. Goldman A (1993) Modern ferrite technology. Marcel Dekker, New York
4. Trivedie BS, Janie NN, Joshi HH, Kulkarni RG (2000) J Mater Sci 3:5523
5. Choni AA, Etyhhand AI, Mohamed AA (1980) Proc Int Conf Ferrites 5:216
6. Ramana Reddy AV, Ranga Mohan G, Boyanov BS, Ravinder D (1999) Mater Lett 39:153
7. Duong GV, Turtelli RS, Hahn N, Linh DV, Reissner M, Michor H, Fidler J, Wiesinger G, Grossinger R (2006) J Magn Magn Mater 307:313
8. Reddy AVR, Mohan GR, Ravinder D, Boyanov BS (1999) J Mater Sci 34:3169
9. Gul IH, Abbasi AZ, Amin F, Anis-Ur-Rehman M, Maqsood A (in press) J Magn Magn Mater
10. Gabal MA, El-Bellihi AA, Ata-Allah SS (2003) Mater Chem Phys 81:84
11. Grosse G (1992) Mos-90, version 2.2, 2nd edn. (Oskar-Maria-Graf-RRing), Munchen
12. Kumar KV, Ravinder D (2002) Mater Lett 52:166
13. Gabal MA, El-Bellihi AA, El-Bahnasawy HH (2003) Mater Chem Phys 81:174
14. George M, Nair SS, John AM, Joy PA, Anantharaman MR (2006) J Phys D: Appl Phys 39:900
15. Wei QM, Li JB, Chen ZJ (2001) J Mater Sci 36:5115
16. Cullity BD (1956) Elements of X-ray diffraction. Wesley Publishing Reading, MA
17. Kulusreshtha SK (1986) J Mater Sci 5:638
18. Smith J, Wijin HP (1959) Ferrites. Wiley, NY
19. Morrison SR (1977) The chemistry and physics of surface. Plenum Press, NY
20. Irkin YP, Turov EA (1957) Sov Phys JETP 33:673
21. Kliger MI (1979) Phys Stat Sol B 79:9
22. Nikumbh AK, Nagawade AV, Tadke VB, Bakare PP (2001) J Mater Sci 36:653
23. Wu CC, Krishanan SK, Marson TO (1981) J Sol State Chem 37:144
24. Maxwell JC (1973) Electrical and magnetic. Oxford University Press, NY
25. Rabinkin IT, Novikova ZI (1960) Izv Acad Nauk, USSR Minsk 146
26. Fukuda Y, Nagata S, Echizenya K (2004) J Magn Magn Mater 279:325
27. Anantharaman MR, Sindhu S, Jagatheesan S, Malini KA, Kurian P (1999) J Phys D: Appl Phys 32:1801